Applied Clay Science 101 (2014) 369–380

Contents lists available at ScienceDirect

Applied Clay Science

journal homepage: www.elsevier.com/locate/clay

Research paper

Approaches to surface complexation modeling of Ni(II) on Callovo-Oxfordian clayrock

Z. Chen [a,b], G. Montavon [a,*], Z. Guo [b], X. Wang [c], S. Razafindratsima [a], J.C. Robinet [d], C. Landesman [a]

[a] Laboratoire SUBATECH, UMR 6457 CNRS-IN2P3/Ecole des Mines de Nantes/PRES UNAM, 4 rue A. Kastler, 44307 Nantes Cedex, France
[b] Radiochemistry Lab, School of Nuclear Science & Technology, Lanzhou University, Lanzhou 730000, China
[c] Institute of Plasma Physics, Chinese Academy of Sciences, P.O. Box 1126, Hefei, Anhui 230031 PR China
[d] ANDRA, Research and Development Division, 1/7 rue Jean Monnet, 92298 Châtenay-Malabry cedex, France

ARTICLE INFO

Article history:
Received 19 November 2013
Received in revised form 26 June 2014
Accepted 3 July 2014
Available online 10 September 2014

Keywords:
Callovo-Oxfordian clayrock
Ni(II)
Adsorption
Bottom-up approach
Spectroscopic analysis

ABSTRACT

Callovo-Oxfordian formation (COX) is as potential host formation for emplacement of long-term nuclear waste repositories in France. The objective of this work is to assess whether a simplified "bottom-up" approach may explain the retention of Ni(II) by the COX considering two levels of 'upscaling': (i) from clay surfaces to rock clay fraction and (ii) from clay fraction to whole rock samples. To this end, Ni(II) adsorption was investigated by batch equilibrium, XPS, and EXAFS techniques on a representative sample extracted at the location where the storage is supposed to be built (clay content of about 50%) and on the corresponding carbonate-free <2 μm fractions. The results showed that a simplified "bottom-up" approach based on published models available for illite and montmorillonite cannot explain Ni(II) adsorption on the <2 μm fraction when the retention is controlled only by surface complexation on the reactive clay edge sites. An operational model based on the generalized composite modeling approach was used instead. The developed model considers an interaction between two Ni(II) species with one type of clay edge sites. The model developed for the clay fraction gives a satisfactory estimation of Ni(II) adsorption data for the representative clayrock sample. Complementary experiments were performed by X-ray photoelectron (XPS) and X-ray absorption (EXAFS) spectroscopies for both clay fraction and raw COX sample at high Ni(II) loadings. Spectroscopic data were characterized by similar fitting parameters considering formation of Ni phyllosilicate. This indicates that the clay fraction governs the retention of Ni(II), as it was concluded from the batch experiments. Complementary adsorption experiments preformed with COX samples having clay contents representative of the variability occurring at the formation scale (*i.e.* 1.5–47% in weight) show that one cannot neglect the retention properties of the non-clay phases, mainly dominated by calcite, when the clay content becomes the minority. Retention values in the range of 60–300 L/kg can finally be given for describing adsorption properties of trace concentrations of Ni(II) for the clay contents representative of the majority of the Callovo-Oxfordian formation.

1. Introduction

Sedimentary clay-rich formations are under investigation in Europe (Callovo-Oxfordian formation (COX) in France, the Boom clay in Belgium and the Opalinus Clay in Switzerland) as potential host formations for emplacement of long-term nuclear waste repositories. These geological formations were selected based on their capacity to limit transfer towards the biosphere of any radioactive elements released from the waste substances, a result of their low permeabilities, low diffusion coefficients and high ion adsorption/exchange capacities. It is therefore important to be able to predict the uptake of radionuclides on host formations under "*in situ*" conditions. This requires measurements of adsorption data in conditions relevant to the real system and the development of adsorption models explaining how macroscopic retention parameters, in particular 'Kd', are affected by the natural variations in formation mineralogy and pore water composition, as well as by perturbations caused by the presence of the waste cells (*e.g.* temperature, alkaline plume).

Theoretically macroscopic adsorption behavior (Kd) should be predictable by a model which includes sufficiently accurate consideration of all important reactions occurring in solution or at the solid/liquid interface with parameters proposed in the thermodynamic databases for model phases/compounds found in the natural system. This so-called "bottom-up" approach generally requires simplifications in system description; *i.e.* only main phases/adsorption sites are considered being responsible for adsorption. The frequently studied case concerns the adsorption of alkali and alkaline-earth cations reacting with clay mineral surfaces by cation-exchange (CE) processes. Given that clayrocks

* Corresponding author. Tel.: +33 2 51 85 84 20; fax: +33 2 51 85 84 52.
E-mail address: montavon@subatech.in2p3.fr (G. Montavon).

http://dx.doi.org/10.1016/j.clay.2014.07.034
0169-1317/

always contain a variety of minerals other than clays (carbonates, tectosilicates…), a first simplification of the bottom-up approach is to consider that the adsorption behavior is governed by the clay fraction (*i.e.* <2 μm). One must then deal with the natural complexity of this operational fraction since it is generally a mixture of different clay minerals (illite, smectite, mixed-layer illite–smectite minerals (I/S), kaolinite …), some of them having as yet uncharacterized exchange constants (case of I/S). As an example, Tournassat et al. (2009) showed that it was still possible to use a "bottom-up" approach to explain the adsorption of major cations on typical COX clayrock considering two reference clay minerals (illite and montmorillonite) and I/S as a mixture of illite and montmorillonite. The modeling is even simpler for trace concentrations of Cs using generic parameters obtained for Cs and illite (Bradbury and Baeyens, 2000). This approach was successfully applied to the Opalinus (Van Loon et al., 2009) and Boom (Maes et al., 2008) clay formations.

However, the adsorption of many metal ions is also governed by surface complexation reactions. These reactions involve formation of inner and outer sphere complexes with mineral surface moieties and, therefore, are inherently potentially much more complex in respect to stoichiometry than the simple electrostatically governed cation exchange phenomena. Applying the "bottom-up" approach is consequently also more complex. To the best of our knowledge, the "bottom-up" approach for metal ions sensitive to both cation exchange and surface complexation reactions has been applied only to the Opalinus clayrock (Bradbury and Baeyens, 2011; Hartmann et al., 2008) using the 2 Site Protolysis Non-Electrostatic Surface Complexation and Cation Exchange adsorption model (2 SPNE SC/CE) initially developed for the Ni(II) + Zn(II)/montmorillonite system (Bradbury and Baeyens, 1997). The agreement between experimental data and the prediction was relatively good when illite and illite–smectite phases were considered responsible for the adsorption and when they were assumed to have the same adsorption properties as pure illite. The bottom-up approach has also been tested for soils contaminated with radionuclides, such as U mill tailings (Davis et al., 1998). These authors showed that the bottom-up approach could not satisfactorily explain measured adsorption data and they proposed representing the observed data using a semi-empirical modeling approach, the so-called Generalized Composite Model (GCM) (Davis et al., 1998, 2004). Their goal was to develop the simplest possible model by using the minimum number of equilibria necessary to fit the adsorption data acquired under field-relevant conditions. The reactions were quantitatively described considering a non-electrostatic model with conditional constants including the acid–base properties of the surface hydroxyl groups. Such an approach has been shown to be an efficient tool for describing metal ion adsorption by complex aluminosilicate mineral assemblages (Tertre et al., 2008).

The objective of the work presented here was to assess whether a simplified "bottom-up" approach may explain Ni(II) retention on COX considering two levels of 'up-scaling' (i) from clay surfaces to the clay fraction and (ii) from clay fraction to COX samples. Ni(II) adsorption is sensitive to both cation exchange and surface complexation reactions and is generally considered as a representative model for divalent cations. Ni(II) has already been extensively studied in adsorption studies on clayrock (Bradbury and Baeyens, 2011) and model clay phases (Bradbury and Baeyens, 1997, 2009; Donat et al., 2005; Echeverría et al., 2003; Elzinga and Sparks, 2001; Gu and Evans, 2007; Hu et al., 2010; Kraepiel et al., 1999; Song et al., 2009; Tertre et al., 2005). Based on the data obtained for Ni(II)/Opalinus clay (Bradbury and Baeyens, 2011), and as was shown for alkali and alkaline-earth cations for COX- (Tournassat et al., 2009), Opalinus- (Van Loon et al., 2009) and Boom- (Maes et al., 2008) clay formation, one considers that Ni(II) adsorption on COX is governed by the clay fraction.

To do this, adsorption data were measured on <2 μm fractions extracted from the COX clayrock and on a reference sample extracted from a place located where the storage is supposed to be built (mean clay content of 50%). The effect of pH, P_{CO2}, Ni(II) concentration and ionic strength on Ni(II) adsorption were studied. The quantitative description of Ni(II) adsorption will be done based on the simplifying approaches proposed in the literature (Bradbury and Baeyens, 2011; Davis et al., 1998). Complementary analyses were done by spectroscopic tools to better understand the role of the clay fraction in Ni(II)/COX retention. Finally, the importance of the clay fraction in the retention will be qualitatively assessed by studying the adsorption of Ni(II) on COX samples with clay contents representative of the variability occurring at the formation scale (*i.e.* 1.5–47% in weight). This will allow to provide a range of Kd values describing Ni(II) adsorption on COX clayrock.

2. Experimental section

2.1. Materials

All solutions were prepared with ultra-pure deionized water (18.2 M Ω cm^{-1}) and with commercially available chemical products of analytical grade or superior. Ni-63 tracer (carrier-free) was provided by CERCA (AREVA NP, France).

2.1.1. COX samples

The mineralogy of the formation consists mainly of phyllosilicates (mainly illite and mixed layer illite/smectite, kaolinite, mica, and chlorite), tectosilicates (mainly quartz and feldspars) and carbonates (mainly calcite and dolomite) (Gaucher et al., 2006). The proportions of these components vary mainly depending on the depth of the sedimentary layer (Fig. 1).

Moreover, the Callovo-Oxfordian formation is characterized by two types of mixed layer illite–smectite. The first occurs in the upper part of the layer and is essentially randomly interstratified R = 0 I/S (I/S_{R0}) with an average smectite/illite proportion of 55/45 whereas the lower part of the layer is ordered R = 1 I/S (I/S_{R1}) and characterized by an average smectite/illite proportion of 35/65 (Gaucher et al., 2004).

In order to assess the first level of up-scaling, from clay surfaces to the clay fraction, two <2 μm clay mineral fractions representing the I/S_{R0} (named R0 in the following) and I/S_{R1} (named R1 in the following), converted to the Na-form, were used. They were isolated from raw core samples according to the protocol given in Claret et al. (2004).

EST26480 sample was used as a reference to study the second level of up-scaling, *i.e.* from clay fraction to COX samples. It was extracted from a place located in the transient zone (UA2 unit) where the storage is supposed to be built. The mineralogy in this zone is relatively homogeneous with a clay content varying between 45 and 55% (Vinsot et al., 2010). In order to study the role of non-argillaceous phases on Ni(II) adsorption, COX core samples having different mineral contents were selected in the upper part of the layer (I/S_{R0}) where mineral content variability is the highest (Fig. 1). Sample characteristics and names are given in Table 1. COX samples were crushed and sieved at 63 μm before used.

2.1.2. Sample characterization

The mineralogy of the studied samples was quantified by a combining X-ray powder diffraction and bulk chemical analysis (Cosenza et al., 2014). Crystalline phases were first determined and roughly estimated from X-ray diffraction (XRD) analysis (Bruker D8 Advance A25 diffractometer–Cu Kα radiation) performed on disoriented powders (<200 μm fraction). Clay minerals were then accurately identified in the <2 μm fraction using X-ray diffraction (XRD) applied to oriented preparations (air-dried and ethylene glycol treatment). Identification of clay minerals was carried out automatically by the program ClayXR (Bouchet, 1992; Lanson and Bouchet, 1995). Additional information (including interstratified clay minerals) was obtained by comparing the experimental results with theoretical diffractograms calculated with the program NEWMOD© (Reynolds, 1980).

The quantitative estimation of the proportion of the different phases is performed by combining chemical analysis of the bulk material with cation exchange capacity (cobalt hexamine chloride method (Rémy

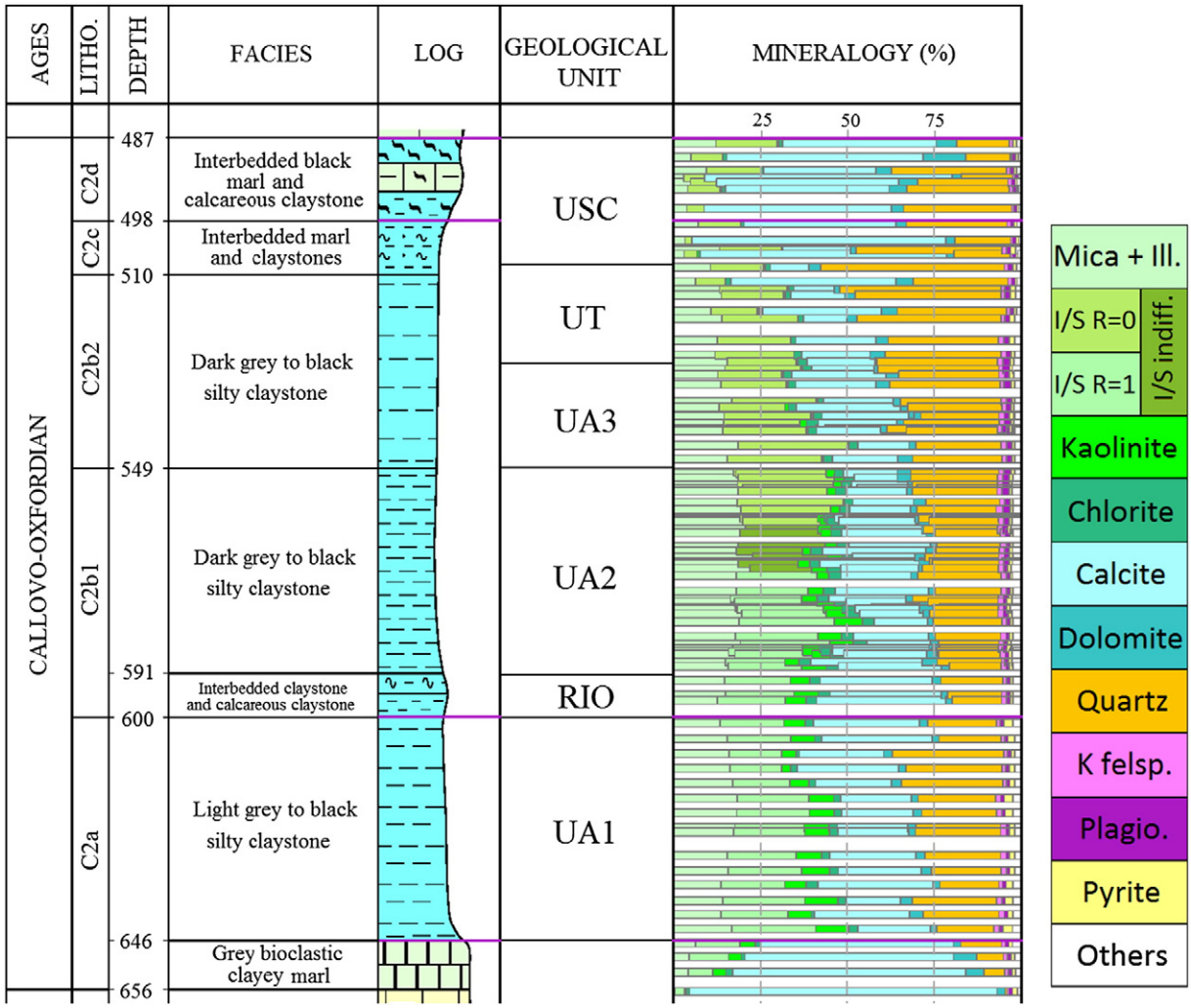

Fig. 1. Mineralogy of COX formation as a function of the depth (EST 423). USC: "Unité Silto Carbonatée" (siltocarbonated unit); UT: "Unité de Transition" (transitional unit) and UA: "Unité Argileuse" (Clayey Unit).

and Orsini, 1976)) and carbonate content measurements (Bernard calcimeter). The method we used is similar to the one published in (Calvert et al., 1989). Chemical analyses were performed by X-ray fluorescence spectrometry taking into account the following elements: Si, Al, Mg, Fe, Ca, Na, K, Mn, Ti and P. From these analyses, mineral content quantification was then obtained by a normative calculation based on the theoretical structural formula of the minerals (Newman and Brown, 1987; Weaver, 1989), for micas, illite and I/S ordered and disordered; for the other minerals (Deer et al., 1992). Cation exchange capacity (CEC) values as well as the carbonate content were allowed to control the calculation results and eliminate some obviously incorrect solutions.

The results, given in Table 1, show an important variation in the mineralogy with notably a clay content varying between 1.5 and 53% (by weight).

2.2. Experimental procedures

All experiments were performed at T = 23 ± 3 °C. The pH values given in the manuscript are measured under equilibrium conditions.

2.2.1. Batch-type adsorption experiments

Ni(II) adsorption was studied as a function of pH, Ni(II) concentration and ionic strength. For the <2 μm fractions, experiments were carried out in non-complexing medium ($NaClO_4$) under different atmospheres (atmospheric conditions $P_{CO2} = 10^{-3.5}$ atm, Ar, N_2:CO_2 99:1) in order to assess the effect of carbonate on retention. For COX samples, experiments were done in the presence of a synthetic pore water (SPW) representative of the COX formation (Gaucher et al., 2007). The solid was systematically pre-equilibrated for about 30 days with the solution before Ni(II) addition. Experiments were done in a glove box with $P_{CO2} = 10^{-2}$ atm to control the carbonate concentration in solution and to limit carbonate phase dissolution/precipitation processes. Note that HCO_3^- species was added to the SPW at the expected concentration in equilibrium with CO_2. Water compositions in equilibrium with the solids are given in Table 2. All adsorption data were realized under conditions where Ni(II) precipitation does not occur before the addition of the clay material (this was checked by filtration at 0.1 μm).

It is important to indicate that, in the present paper, we are interested in studying the adsorption process which is generally considered as rapid. Preliminary experiments showed that a contact time of 3 days was necessary to reach "equilibrium" conditions. However, it is well known that slower uptake by incorporation may occur with time on calcite (Lakshtanov and Stipp, 2007). This potential long-term retention was not specifically studied in the present study. The solid and liquid phases were separated by centrifugation at 15,000 ×g for 30 min.

Table 1
Characteristics of samples used in the present study (units are in percentage, if not otherwise indicated).

Sample	EST05632–EST05688[a]	Enriched clay fraction R1	EST26480	EST27861	EST27862
Drilling	EST 205	EST 423	FOR 1118	EST 423	EST 423
Depth (m)	474.9–489.1	–	490	501.3	455
Lithofacies	C2b1	–	C2b1	C2c	C2c
Geological unit	UA3	–	UA3	USC1	USC1
Layer part	R = 0	R = 1	Transition zone R = 0/R = 1[b]	R = 0	R = 0
Quartz + opale	21	4–7	17–23	37–42	9–12
Calcite	13	–	18–23	27–40	84–86
Dolomite, ankerite	12	–	1–6	2–5	–
Feldspath-K	4	0–1	>0–4	1–3	0–2
Plagioclase	2	–	–	–	–
Pyrite	1.7	–	>0–1.5	>0–2	0–1
Iron phases (Siderite, Hematite, …)	–	0–4	0–3	0–2	–
TiO_2	1.4	0–1	0–0.7[c]	0–0.2[c]	–
Clay minerals					
Illite[d]	20	15–22	14–29	5–11	–
I–S	23	40–51	18–33	4–10	0–3[e]
Kaolinite	–	18–25	0–6	–	–
Chlorite	2	1–4	0–6	0–3	–
Masses (in g per kg of sample) used for model 2 (CE + SC)					
Illite	668	481	330	112	6.8
Montmorillonite	278	159	140	38.5	8.3
Masses (in g per kg of sample) used for model 1 and the GCM					
Reactive phase	945	640	470	150	15
Cation exchange capacity (eq/kg)					
Measured value	0.44	0.34	0.18	0.08	0.015
Calculated value	0.29–0.44[f]	0.19–0.25	0.12–0.23	0.03–0.07	0–0.017

[a] Composition of the raw samples from which the enriched clay fraction R0 was extracted (Tournassat et al., 2007); the mass and the CEC values were calculated for R0 using the composition given in the column and considering that 99% of the enriched clay fraction corresponds to the clay minerals (Tournassat et al., 2009).
[b] I/S_{R0} characteristics were used for the modelling.
[c] Not observed by XRD.
[d] Mica, illite and I/S with more than 90% in illite.
[e] Percentage calculated from the measured CEC ($1.5.10^{-2}$ eq/kg) supposed to be associated with a small amount of phyllosilicates not detected by XRD.
[f] Clay content uncertainties of 20% were considered for the calculation (Gaucher et al., 2004).

The distribution coefficient of Ni(II) (Kd in L/kg) was calculated according to the following equation:

$$Kd = \frac{q}{Ceq} = \frac{(A0 - Aeq)}{Aeq} \cdot \frac{V}{m} \quad (1)$$

where q (mol/kg) is the amount of Ni(II) adsorbed, Ceq (mol/L) the aqueous Ni(II) concentration, A_0 the activity measured in the suspension, A_{eq} the activity measured in the aqueous phase, V (L) the volume of aqueous solution and m (kg) the mass of the sorbent.

MES (2-(*N*-morpholino) ethanesulfonic acid) and MOPS (3-(*N*-morpholino) propanesulfonic acid) (2.10^{-3} mol/L) buffers were used

Table 2
Water composition after equilibrium with the solid phases before Ni(II) addition. Mean values are reported in the table; the deviation does not exceed 13% as compared to the water composition before contact with the material and from one system to the other.

Material		R0	R0/R1	COx samples
pH		4.64	3–10	7.4
pCO_2 (bar)		$10^{-3.5}$	0, $10^{-3.5}$,10^{-2}	10^{-2}
Solid-to-liquid ratio (g/L)		10	5	1–10
Performed experiments		Naturally-occuring minor elements	Sorption (pH-edge, isotherm, reversibility)	Sorption isotherm naturally-occuring minor elements
Dissolved components		Concentration (M)		
Major ions	Na	0.1	0.1	$4.6.10^{-2}$
	K	n.m.	n.m.	1.10^{-3}
	Mg	n.m.	n.m.	$6.7.10^{-3}$
	Ca	n.m.	n.m.	$7.4.10^{-3}$
	Sr	n.m.	n.m.	2.10^{-4}
	Cl	n.m.	n.m.	$4.1.10^{-2}$
	ClO_4	0.1	0.1	–
	SO_4	n.m.	n.m.	$1.6.10^{-2}$
Minor elements	Co	$4.9.10^{-9}$	n.m.	$3.9.10^{-8}$
	Zn	$3.1.10^{-8}$	n.m.	$1.65.10^{-8}$
	Ni	1.10^{-8}	n.m.	$1.45.10^{-7}$
	Mn	5.10^{-8}	n.m.	6.10^{-7}
	Fe	$<10^{-6}$	n.m.	$<10^{-6}$

n.m.: not measured.

to keep the pH constant for adsorption isotherms measured at pH 6.5 and 7.4, respectively.

2.2.2. Desorption experiments

Desorption experiments were done with the <2 μm fraction to assess retention process reversibility. It was performed after the adsorption phase in two ways. For the experimental data corresponding to the adsorption isotherms in concentration, about three quarter of the aqueous phase was removed and replaced by the solution free of Ni (the term "dilution" will be used throughout the text to refer to this way). For the adsorption data measured as a function of the pH, the pH was decreased by one unit. The suspension was then allowed to re-equilibrate before separation and analysis. In all cases, the re-equilibrium time was set arbitrary to 30 days. The method was also used to determine the amount of naturally-occurring Ni(II) and other divalent elements which could compete with added Ni(II) for adsorption sites (Fe(II), Zn(II), Co(II), Mn(II)).

2.2.3. Analytical tools

Analyses of radioactive nickel (^{63}Ni) were performed by liquid scintillation counting with a Packard 3170 TR/SL liquid scintillation analyzer using an Ultima Gold LLT®(Packard) scintillation mixture. Stable trace elements were analyzed by ICP-MS (Thermo Electron Xseries 2). Solution composition was determined by ionic chromatography (Dionex ICS1000) measurements.

2.3. Modeling Ni(II) adsorption

Our objective was to quantitatively describe Ni(II) adsorption on the <2 μm fraction and then to use the model to predict adsorption on full complexity COX samples. Reactions occurring in the aqueous phase were calculated using the thermodynamic database THERMOCHIMIE (Duro et al., 2012) which was completed with constants given in the literature (Table 3). All calculations were done with the PHREEQC code (version 2.15) (Parkhurst and Appelo, 1999) and the Davies equation (Davies, 1962) was used to account for the ionic strength correction for solutes.

We have considered two approaches. The first one corresponds to the one applied to model adsorption data of metal ions on Opalinus Clay (Bradbury and Baeyens, 2011), *i.e.* (i) illite and I/S are the reactive phases and (ii) I/S reactivity corresponds to that of illite for both the surface complexation and the cation exchange reactions. It will be called "model 1" throughout the paper. The second approach, referred to "model 2"; it also considers assumption (i) but describes I/S as a combination of illite and montmorillonite (Tournassat et al., 2009). In this model, the amounts of the reference clays, illite (m_{Illite}) and montmorrilonite ($m_{mont.}$), were calculated considering the weight amount of illite and I/S measured in the samples and the average smectite/illite proportions given in Section 2.1.1 for I/S_{R0} and I/S_{R1} (see Table 1). Model 2 is described below.

2.3.1. Model 2, cation exchange (model 2, CE)

Cation exchange capacities are given in Table 1. They originate mainly from two clay minerals illite and I/S. Cation exchange sites are located on illite basal and I/S interlayer and basal surfaces. In this model, generic CEC values of 0.16 eq/kg and 0.9 eq/kg were considered for illite (Bradbury and Baeyens, 2000) and montmorillonite (Robert, 1996), respectively. CEC values were thus recalculated from the respective content of illite (m_{illite}) and smectite ($m_{smectite}$) and their theoretical CEC values according to the relation:

$$CEC = m_{illite} \cdot CEC(illite) + m_{mont.} \cdot CEC(montmorrilonite) \quad (2)$$

The obtained values are reported in Table 1. A good agreement between experimental and calculated values is observed with, however, a slight underestimation of the calculated value for the R1 < 2 μm fraction. This might be explained by local heterogeneities or a significant contribution of kaolinite to the CEC (present in a significant amount in the sample). Indeed, kaolinite may contain smectite layer impurities on its crystal surfaces generating additional cation exchange sites (MA and EGGLETON, 1999). In the absence of further information, kaolinite was not considered in the modeling. The exchange constants are known to vary according to the exchanger composition (Tournassat et al., 2009). Constants were thus selected depending on the system being studied (SPW or 0.1 M $NaClO_4$) and are given in Table 4 following the Gaines–Thomas convention (Gaines and Thomas, 1953).

2.3.2. Model 2, Surface complexation (model 2, SC)

Several surface complexation models are available in the literature for illite (Bradbury and Baeyens, 2009; Echeverría et al., 2003; Elzinga and Sparks, 2001; Gu and Evans, 2007; Hu et al., 2010) and for smectite (Bradbury and Baeyens, 1997; Donat et al., 2005; Kraepiel et al., 1999; Song et al., 2009; Tertre et al., 2005). These models are able to describe experimental data covering a wide range of experimental conditions (pH, ionic strength, metal ion concentration). However, there are no generic parameters available for both illite- and smectite-type clay minerals. Although similar surface species were considered, the constants describing the surface complex reactions are quite different from one model to another. The reason for this is that the constants deduced from the modeling are not only strongly dependent on the surface

Table 3
Constants used to describe Ni(II) and competing divalent metal ion speciation in aqueous solution. Otherwise indicated, the constants are taken from (Duro et al., 2012).

Aqueous species	Reaction	logK				
		Ni(II)	Zn(II)	Co(II)	Mn(II)	Fe(II)
$M(OH)^+$	$M^{2+} + H_2O \Leftrightarrow \equiv M(OH)^+ + H^+$	−9.54	−8.96[a]	−9.23	−10.59	−9.5
$M(OH)_2$	$M^{2+} + 2H_2O \Leftrightarrow \equiv M(OH)_2 + 2H^+$	−18	−16.9[a]	−18.6	−22.2	−20.6
$M(OH)_3^-$	$M^{2+} + 3H_2O \Leftrightarrow \equiv M(OH)_3^- + 3H^+$	−29.4	−28.4[a]	−31.7	−34.8	−31.9
$M(OH)_4^{2-}$	$M^{2+} + 4H_2O \Leftrightarrow \equiv M(OH)_4^{-2} + 4H^+$	–	–	−46.42	−48.3	−46
MCO_3	$M^{2+} + CO_3^{2-} \Leftrightarrow \equiv MCO_3$	4.2	–	4.23	6.5	7.45
$M(CO_3)_2^{2-}$	$M^{2+} + 2CO_3^{2-} \Leftrightarrow \equiv M(CO_3)_2^{2-}$	6.2	–	–	–	5.69
$MHCO_3^+$	$M^{2+} + H^+ + CO_3^{2-} \Leftrightarrow \equiv MHCO_3^+$	11.73	–	12.22	11.61	11.77
$MOHCO_3^-$	$M^{2+} + H_2O + CO_3^{2-} \Leftrightarrow \equiv MOHCO_3^- + H^+$	–	–	–	–	−4.03
MSO_4	$M^{2+} + SO_4^{2-} \Leftrightarrow \equiv MSO_4$	2.35	–	2.3	2.25	2.2
$M(SO_4)_2^{2-}$	$M^{2+} + 2SO_4^{2-} \Leftrightarrow \equiv M(SO_4)_2^{2-}$	3.01	–	–	–	–
$MHSO_4^+$	$M^{2+} + H^+ + SO_4^{2-} \Leftrightarrow \equiv MHSO_4^+$	–	–	–	–	3.07
$M(Cl)^+$	$M^{2+} + Cl^- \Leftrightarrow \equiv M(Cl)^+$	0.4[b]	–	0.57	0.3	0.14
$M(Cl)_2$	$M^{2+} + 2Cl^- \Leftrightarrow \equiv M(Cl)_2$	0.96[b]	–	0.02	0.25	−0.52
$M(Cl)_3^-$	$M^{2+} + 3Cl^- \Leftrightarrow \equiv M(Cl)_3^-$	–	–	−1.71	−0.31	1.02
$M(Cl)_4^{2-}$	$M^{2+} + 4Cl^- \Leftrightarrow \equiv M(Cl)_4^{-2}$	–	–	−2.09	–	–

[a] Taken from Bradbury and Baeyens (1997).
[b] Taken from Hummel et al. (2002).

Table 4
Parameters used to describe the ion exchange process. The masses of the reference minerals used for the modeling are given in Table 1.

Mineral of reference	Site types	Site capacities (meq/kg)	Reference
Illite	Planar sites	160	Bradbury and Baeyens (2000)
Montmorillonite		900	Robert (1996)

	Cation exchange reaction	Experiments realized in 0.1 M $NaClO_4$	Experiments realized in SPW	
		Exchange constants (log K)	Exchange constants (log K)	Reference
Illite	Ni^{2+} + 2Na-X Ni-X2 + $2Na^+$	1.1	1.1	Bradbury and Baeyens (2009)
	Co^{2+} + 2Na-X Co-X2 + $2Na^+$	1.3	1.3	
	K^+ + Na-X K-X + Na^+	Not considered	1.2	Gaucher et al. (2009)
	Ca^{2+} + 2Na-X Ca-X2 + $2Na^+$	Not considered	0.7	
	Mg^{2+} + 2Na-X Mg-X2 + $2Na^+$	Not considered	0.7	
	Fe^{2+} + 2Na-X Fe-X2 + $2Na^+$	Not considered	0.7	
	Sr^{2+} + 2Na-X Sr-X2 + $2Na^+$	Not considered	0.7	
	Mn^{2+} + 2Na-X Mn-X2 + $2Na^+$	1.1	1.1	Fixed to the one of Ni
	Zn^{2+} + 2Na-X Zn-X2 + $2Na^+$	1.1	1.1	
Montmorillonite	Ni^{2+} + 2Na-X Ni-X2 + $2Na^+$	0.49	0.49	Bradbury and Baeyens (1997)
	Zn^{2+} + 2Na-X Zn-X2 + $2Na^+$	0.59	0.59	
	Co^{2+} + 2Na-X Co-X2 + $2Na^+$	0.57	0.57	Value selected in Bradbury and Baeyens (2005b)
	Mn^{2+} + 2Na-X Mn-X2 + $2Na^+$	0.49	0.49	Fixed to the one of Ni
	K^+ + Na-X K-X + Na^+	Not considered	1.1	Gaucher et al. (2009)
	Ca^{2+} + 2Na-X Ca-X2 + $2Na^+$	Not considered	0.6	
	Mg^{2+} + 2Na-X Mg-X2 + $2Na^+$	Not considered	0.6	
	Fe^{2+} + 2Na-X Fe-X2 + $2Na^+$	Not considered	0.9	
	Sr^{2+} + 2Na-X Sr-X2 + $2Na^+$	Not considered	0.3	

reactions, but also on the sorbent's description, such as site types, site capacities and protolysis constants and whether or not an electrostatic term is considered.

In order to model Ni(II) adsorption, we have selected a "bottom-up" surface complexation adsorption model able to satisfy two main constraints: (i) a similar type of model for the two minerals (*i.e.* same approach to describe the electrostatic term) and (ii) a multi-species model which includes the adsorption of possible competing cations present in the solution. Based on these considerations, and to allow a simple comparison with the prediction made with model 1, it was decided to use the two site protolysis non-electrostatic surface complexation model (2SPNE SC model) (Bradbury and Baeyens, 1997) which describes the adsorption of a series of cations (valence +2 to +4) on both illite and montmorillonite. The parameters used for the modeling are given in Table 5.

2.4. Spectroscopic data

The objective of using spectroscopy is to check the basic assumption of the simplified "bottom-up" approach, *i.e.* the clay fraction dominates Ni(II) retention on COX. In order to do this, two samples were used, the <2 μm fraction R0 and the reference COX sample (EST26480). Ni(II) interaction was studied at the molecular level with spectroscopic tools sensitive to metal ion environment, *i.e.* X-ray photoelectron (XPS) and X-ray absorption (XAS) spectroscopy. It is important to indicate that we were not interested in a thorough characterization of surface species but rather in qualitatively comparing the results and in attempting a quantitative analysis based on published data.

Samples were prepared so as to have a sufficiently high Ni(II) adsorption density on the surface (0.05 mol/L in the presence of 5 g/L of the material at pH ~6.7 and 1% P_{CO2}). Note that the metal ion loading is significantly higher than those studied by the batch technique. This point will be further discussed in the "results and discussion" part. After a contact time of 3 days, the solids were filtered, washed and stored as wet pastes. Ni(II) loadings of 147 ppm and 70 ppm were obtained by modelling for R0 and EST26480, respectively.

2.4.1. XPS measurements

The $Ni_{2p3/2}$ spectra were acquired on an XPS KRATOS AXIS ULTRA electron spectrometer working in fixed analyzer transmission (FAT) mode. The source of photons was an Al monochromatic X-ray source emitting an incident X-ray beam at 1486.7 eV with a FWHM (full-width half-maximum) of 0.25 eV. The sample, fixed on a metallic plate, was analyzed in a chamber under $5 * 10^{-7}$ Pa vacuum. The $Ni_{2p3/2}$ photopeaks were recorded at constant pass energy of 20 eV. The angle-resolved XPS spectra were fitted using a Gaussian–Lorentzian (G-L) peak shape (G-L ratio = 30%) with a Shirley baseline as background. The binding energy uncertainty amounts to 0.3 eV.

2.4.2. EXAFS measurements

Ni K-edge X-ray absorption spectra were recorded at 8333 eV at the National Synchrotron Radiation Laboratory (NSRL, Hefei, China) in fluorescence modes. The electron storage ring was operated at 0.8 GeV with a maximum beam current of 200 mA. The X-ray energy was tuned by using a fixed-exit double-crystal Si (1 1 1) monochromator. Higher order harmonics were suppressed by detuning the monochromator by 25%. The monochromator position was calibrated by assigning the first inflection point to the K-absorption edge of metallic nickel foil at 8333.0 eV. Fluorescence spectra were collected using a multi-element pixel high purity Ge solid-state detector. Scans were collected in triplicate and averaged to improve the signal-to-noise ratio. IFEFFIT and its graphical interfaces ATHENA and ARTEMIS (Ravel and Newville, 2005) were used for background subtraction and fitting. The theoretical scattering phases and amplitudes used in data analysis were calculated with the scattering code FEFF7 (Ankudinov and Rehr, 1997) using the crystal structure of β-$Ni(OH)_2$ and Ni-Talc (Dähn et al., 2002). The fitting procedure followed the one proposed by Dähn et al. (2002); the R values were accurate at ±0.02 Å for R_{Ni-O} and ±0.03 Å for R_{Ni-Ni} and R_{Ni-Si}. The accuracy of N values is ±0.5 for whole shells (Dähn et al., 2002; Scheidegger et al., 1998).

3. Results and discussion

3.1. Ni(II) adsorption on <2 μm fractions: experimental data

3.1.1. Adsorption data

Adsorption data measured for the R0 and R1 samples as a function of pH, P_{CO2}, ionic strength and Ni(II) concentrations are presented in Figs. 2, 3 and 4. As observed for the reference clay minerals, the adsorption at low pH is dominated by the cation exchange mechanism which is

Table 5
Parameters used to describe the surface complexation process. The masses of the reference minerals used for the modeling are given in Table 1.

Model	Reference mineral	Site types	Site capacities (mmol/kg)	Reference
Model 2	Montmorillonite	$\equiv S^sOH$	2	Bradbury and Baeyens (1997)
		$\equiv S^{w1}OH$	40	
		$\equiv S^{w2}OH$	40	
		Surface complexation reactions	$\log K_{int}$	–
		$\equiv S^sOH + H^+ \Leftrightarrow \equiv S^sOH_2^+$	4.5	Bradbury and Baeyens (1997)
		$\equiv S^sOH \Leftrightarrow \equiv S^sO^- + H^+$	−7.9	
		$\equiv S^{w1}OH + H^+ \Leftrightarrow \equiv S^{w1}OH_2^+$	4.5	
		$\equiv S^{w1}OH \Leftrightarrow \equiv S^{w1}O^- + H^+$	−7.9	
		$\equiv S^{w2}OH + H^+ \Leftrightarrow \equiv S^{w2}OH_2^+$	6	
		$\equiv S^{w2}OH \Leftrightarrow \equiv S^{w2}O^- + H^+$	−10.5	
		$\equiv S^sOH + Ni^{2+} \Leftrightarrow \equiv S^sONi^+ + H^+$	−0.6	
		$\equiv S^sOH + Ni^{2+} + H_2O \Leftrightarrow \equiv S^sONiOH + 2H^+$	−10	
		$\equiv S^sOH + Ni^{2+} + 2H_2O \Leftrightarrow \equiv S^sONi(OH)_2^- + 3H^+$	−20	
		$\equiv S^{w1}OH + Ni^{2+} \Leftrightarrow \equiv S^{w1}ONi^+ + H^+$	−3.3	
		$\equiv S^sOH + Zn^{2+} \Leftrightarrow \equiv S^sOZn^+ + H^+$	1.6	
		$\equiv S^sOH + Zn^{2+} + H_2O \Leftrightarrow \equiv S^sOZnOH + 2H^+$	−7.4	
		$\equiv S^sOH + Zn^{2+} + 2H_2O \Leftrightarrow \equiv S^sOZn(OH)_2^- + 3H^+$	−17	
		$\equiv S^{w1}OH + Zn^{2+} \Leftrightarrow \equiv S^{w1}OZn^+ + H^+$	−2.7	
		$\equiv S^sOH + Mn^{2+} \Leftrightarrow \equiv S^sOMn^+ + H^+$	−0.6	
		$\equiv S^sOH + Mn^{2+} + H_2O \Leftrightarrow \equiv S^sOMnOH + 2H^+$	−11	
		$\equiv S^sOH + Co^{2+} \Leftrightarrow \equiv S^sOCo^+ + H^+$	−0.9	
	illite	$\equiv S^sOH$	2	Bradbury and Baeyens (1997)
		$\equiv S^{w1}OH$	40	
		$\equiv S^{w2}OH$	40	
		Surface complexation reactions	$\log K_{int}$	–
		$\equiv S^sOH + H^+ \Leftrightarrow \equiv S^sOH_2^+$	4	Bradbury and Baeyens (2009)
		$\equiv S^sOH \Leftrightarrow \equiv S^sO^- + H^+$	−6.2	
		$\equiv S^{w1}OH + H^+ \Leftrightarrow \equiv S^{w1}OH_2^+$	4	
		$\equiv S^{w1}OH \Leftrightarrow \equiv S^{w1}O^- + H^+$	−6.2	
		$\equiv S^{w2}OH + H^+ \Leftrightarrow \equiv S^{w2}OH_2^+$	8.5	
		$\equiv S^{w2}OH \Leftrightarrow \equiv S^{w2}O^- + H^+$	−10.5	
		$\equiv S^sOH + Ni^{2+} \Leftrightarrow \equiv S^sONi^+ + H^+$	0.7	
		$\equiv S^sOH + Ni^{2+} + H_2O \Leftrightarrow \equiv S^sONiOH + 2H^+$	−8.2	
		$\equiv S^sOH + Ni^{2+} + 2H_2O \Leftrightarrow \equiv S^sONi(OH)_2^- + 3H^+$	−17.3	
		$\equiv S^{w1}OH + Ni^{2+} \Leftrightarrow \equiv S^{w1}ONi^+ + H^+$	−1.8	Bradbury and Baeyens (2011)
		$\equiv S^sOH + Co^{2+} \Leftrightarrow \equiv S^sOCo^+ + H^+$	0	Bradbury and Baeyens (2009)
		$\equiv S^sOH + Co^{2+} + H_2O \Leftrightarrow \equiv S^sOCoOH + 2H^+$	−7	
		$\equiv S^sOH + Co^{2+} + 2H_2O \Leftrightarrow \equiv S^sOCoZn(OH)_2^- + 3H^+$	−16.5	
		$\equiv S^sOH + Zn^{2+} \Leftrightarrow \equiv S^sOZn^+ + H^+$	0.98[a]	This work
		$\equiv S^sOH + Mn^{2+} \Leftrightarrow \equiv S^sOMn^+ + H^+$	−0.24[a]	This work
GCM		$\equiv SOH$	40	This work
		Surface complexation reactions	$\log K$	
		$\equiv SOH + Ni^{2+} \Leftrightarrow \equiv SONi^+ + H^+$	−2.9	
		$\equiv SOH + Ni^{2+} + H_2O \Leftrightarrow \equiv SONiOH + 2H^+$	−12.5	

[a] Constants determined using linear free energy relationships.

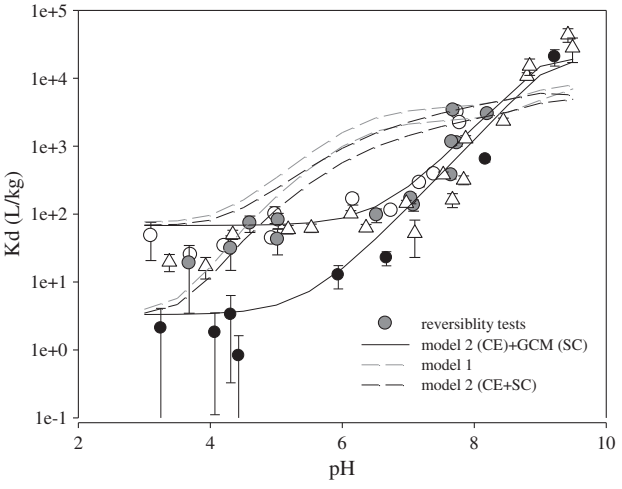

Fig. 2. Ni(II) adsorption on R0 as a function of pH for two ionic strengths under Ar atmosphere. S/L = 5 g/L. (○) [Ni] = $5.7 * 10^{-6}$ M, 0.1 M $NaClO_4$; (△) [Ni] = $4.8 * 10^{-6}$ M, 0.1 M $NaClO_4$; (●) [Ni] = $4.8 * 10^{-6}$ M, 0.4 M $NaClO_4$. The lines correspond to the tested model with parameters given in Tables 1, 3, 4 and 5. The reversibility test was done following a pH perturbation.

independent on pH but strongly depends on the ionic strength: the higher the ionic strength, the greater the competition for exchange sites and the lower the adsorption. Above pH = 5, the increase in adsorption is explained by surface complexation reactions between Ni(II) and surface hydroxyl groups leading to proton exchange. In this case, the ionic strength is less important, as observed experimentally. Finally, the Kd values decrease as the Ni(II) concentration increases (Fig. 2), as expected by the principle of site saturation. It can be noted that this behavior is incompatible with a surface precipitation process. However, one cannot exclude this occurs after the adsorption process, surface precipitates are formed with time according to the Ni concentration, as it was observed for various clay minerals (Dähn et al., 2002; Scheidegger et al., 1998). Such a possibility will be evaluated by the spectroscopic tools.

It is important to indicate that the 2 SPNE SC model used in the "bottom-up" does not consider the possible formation of ternary surface complexes with complexing agents like the carbonate ions which are present in the COX pore water in significant amount. The carbonate effect was experimentally studied to assess its potential role on the adsorption. As observed in Fig. 3, no significant difference in the Kd value was observed between the experiments realized under ambient (0.031% CO_2), Ar or 1% CO_2 atmospheres. This appears consistent with the low percentage, *i.e.* below 3%, of Ni carbonato complexes

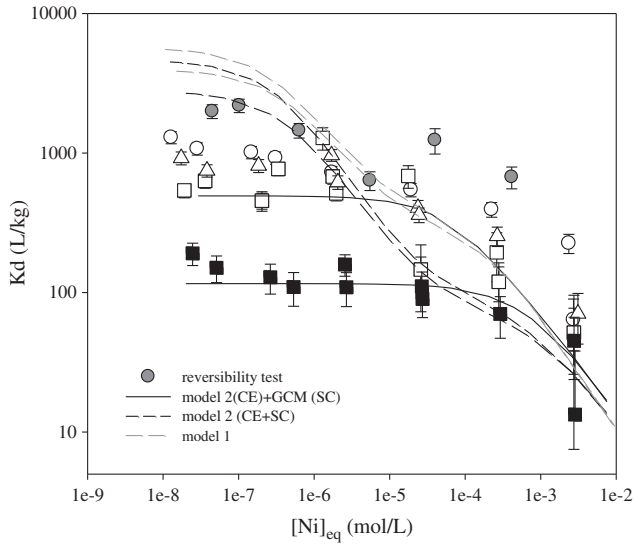

Fig. 3. Ni(II) adsorption on R0 for different atmospheres and different pH values; effect of Ni(II) concentration; S/L = 5 g/L, 0.1 M $NaClO_4$. (O) pH = 7.4, Ar atmosphere; (Δ) pH = 7.4 1% CO_2; (□) pH = 7.4, ambient atmosphere (■) pH = 6.4, Ar atmosphere; The lines correspond to the tested models. The reversibility test (gray symbols) was made according to the dilution method. The lines correspond to the tested model with parameters given in Tables 1, 3, 4 and 5.

calculated for the near neutral pH conditions expected for the COX formation.

The adsorption processes are described based on the law of mass action considering the equilibrium principle. The reversibility tests are presented in Figs. 2 and 3 (gray symbols). When reversibility was tested by a pH change (Fig. 2), the principle of reversibility is valid, *i.e.* Kd values derived from adsorption and desorption tests are identical. However, a desorption hysteresis was observed in the adsorption/desorption experiments performed at constant pH by dilution (Fig. 3). Such a hysteresis would be explained by a slower desorption kinetic rate than the contact time fixed for the experiment, *i.e.* 30 days (see Section 2.2.2).

Finally, it is worth saying that the adsorption affinity for Ni(II) between R0 and R1 samples is similar (Fig. 4) over the entire pH range studied. This is quite surprising because the difference in the various clay phase contents is significant (Table 1): (i) the ratio between the mass of I/S and the mass of illite is close to one for R0 but higher for R1 (~2) and (ii) a high content of kaolinite was quantified for R1 whereas it was not observed in R0. Assuming that the site concentrations are similar for R0 and R1, these results suggest that similar surface hydroxyl sites (in term of affinity constants) are present at the surface of the clay minerals, or at least that the difference in affinity is not significant enough to be observed for the clay fraction of the COX samples under the studied experimental conditions.

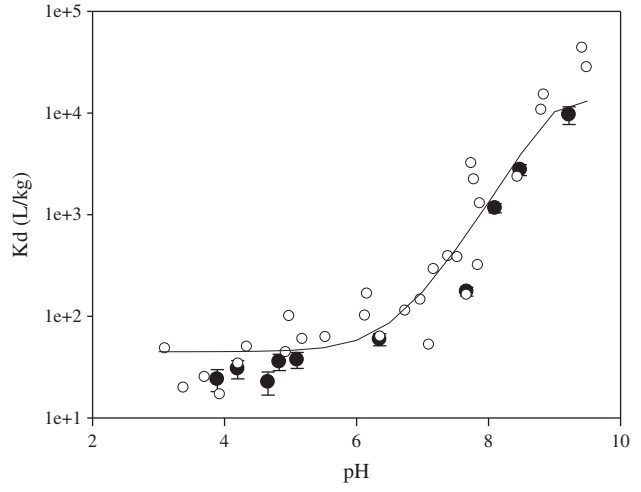

Fig. 4. Ni(II) adsorption on R1 as a function of pH under Ar atmosphere. S/L = 5 g/L, 0.1 M $NaClO_4$, [Ni] = $4.8 * 10^{-6}$ M. The open symbols represent the data obtained with R0 under similar conditions (see Fig. 2). The line corresponds to the tested model with parameters given in Tables 1, 3, 4 and 5 (GCM model).

3.1.2. "Naturally occurring" elements

Trace elements present in the COX formation, and more particularly divalent metal ions (Bradbury and Baeyens, 2005a), can compete with Ni(II) for surface hydroxyl groups. Zn(II) is particularly important; it has a strong competitive effect on Ni(II) adsorption on Na-montmorillonite (Bradbury and Baeyens, 1997) and it is present in relative high amounts in the COX formation (Gaucher et al., 2004). At the depth from which the R0 sample was extracted (borehole EST205, lithofacies C2B1, I-S R0), the Zn content of the rock amounts to 85–117 ppm.

Although metal ions may compete for adsorption sites, the competition effect should remain limited: (i) the vast majority of the inventory is not exchangeable because it is incorporated in minerals and (ii) the exchangeable fraction may be removed through different treatments used in order to separate <2 μm fraction. However, for the sake of completeness, it was decided to include the competition effect in the modelling for R0.

Naturally-occurring metal ions are present at trace concentrations in the formation and are expected to interact mainly with the surface sites by complexation. This exchangeable part was assessed by equilibrating the suspension at a pH where the adsorption by surface complexation is weak (Fig. 2) *i.e.* pH = 4.6. In spite of some treatments to extract/purify the clay fraction (Claret et al., 2004), "naturally occurring" elements, notably divalent cations Ni(II), Co(II), Zn(II), Mn(II) are still observed in the solution (Table 2). Note that a part of these elements may also come from the product ($NaClO_4$) used for preparing the solution (Table 2).

3.2. Modeling adsorption on the <2 μm fraction; from clay surfaces to the clay fraction

3.2.1. The "bottom-up" approach

The first objective was to use model 2 to describe the adsorption behavior of the "naturally occurring" elements with the goal to determine the exchangeable part which has to be considered for the competition effects. Since the ions are present at trace concentrations, and the pH is equal to 4.64 metal uptake occurs mainly on strong and exchange type sites. For the surface complexation constants on strong sites, data exists for montmorillonite (Co(II), Mn(II), Zn(II), Ni(II)) but only the constants describing Co(II) and Ni(II) interaction with illite are given in the literature. An estimation of the constants for the strong site binding of Zn(II) (1.06) and Mn(II) (−0.7) was estimated using linear free energy relationships (Bradbury and Baeyens, 2005b) considering the formation of the surface complex ≡ S–OM^+ (the dominating species at the pH studied). Using the constants reported in Tables 4 and 5, and considering that the concentrations of the divalent cations measured in solution are in equilibrium with R0, it is possible to estimate the amount of elements interacting with the surface and which can compete with Ni introduced in the system: 0.96, 0.22, 0.03 and 0.1 ppm for Zn(II), Mn(II), Co(II) and Ni(II) respectively. The exchangeable part of the naturally occurring elements represents less than 5% of the overall inventory in the extracted clay fraction. The values given above are taken into account in the calculation presented below.

Model 2 can describe the adsorption data relatively well when the ion exchange adsorption mechanism dominates retention (pH <5) (Fig. 2). This result is consistent with the results obtained with cations where the adsorption is governed by a cation exchange mechanism (Tournassat et al., 2009). The agreement is not good beyond pH 5,

i.e. the area in which surface complexation mechanisms govern the retention. The model (dotted line) does not reproduce the curve Kd = f(pH): it overestimates the adsorption between pH 5 and 8, and underestimates the retention beyond pH 8. A similar result was obtained without considering a competition with "naturally occurring" trace elements (data not shown) indicating that under the studied conditions, the predicted competition is not important. For the isotherms, the agreement is relatively good for highest concentrations of Ni(II) indicating that the content of sites present in high amounts is well reproduced (cation exchange and weak site capacities).

Similar results were obtained with model 1 with however a better description of the isotherms for the highest metal ion concentration (5.10^{-6} M < $[Ni]_{eq.}$ < 10^{-3} M) (Fig. 3).

These results indicate that the 2SPNE SC model cannot properly predict the surface complexation mechanism. Given the large number of equilibria (acid–base and surface complexation constants) and the absence of error estimations associated with these constants in the literature, it was not possible to modify the parameters in a reasonably constrained fashion in order to get a better agreement.

3.2.2. The generalized composite model

As the "bottom-up" approach based on the 2SPNE SC model is not able to reproduce Ni(II) adsorption on the COX <2 μm fraction, the generalized composite model was tested as a second approach for describing the surface complexation reactions. Such a simplification has been demonstrated to be an efficient method for describing rare earth element adsorption by complex aluminosilicate mineral assemblages (Tertre et al., 2008). Based on the previous results, the competition effect modelled with published parameters was not important in the Ni concentration range studied. The competition between Ni(II) and natural elements for surface sites was assumed not significant in the GCM. Following the approach of Tournassat et al. (2009) and the relatively good agreement obtained between the experimental data and the prediction, model 2 was used for modeling the exchange reactions (see Section 2.3.1)

The methodology is to start with what is known:

1. Following the work of Bradbury and Baeyens (Bradbury and Baeyens, 2011), it was decided to consider only a single reactive phase. The basic difference is that this phase does not correspond to a defined clay phase but must be viewed as a mixture of clay phases presenting surface hydroxyl sites of similar affinity for Ni. The close adsorption properties of R1 and R0 with respect to Ni support this hypothesis.
2. $Ni(OH)_i^{2-i}$ (with i = 0–2) species interact with surface sites. In a first approach, the amount of sites was fixed equal to the number of weak sites derived from the 2 SPNE SC model, as this model was able to roughly represent Ni(II) adsorption for the highest Ni(II) concentrations (Fig. 3).

At least two surface complexation reactions had to be considered using the constants given in Table 5 in order to reach a good agreement between the experiment and the calculation. The surface complex species ≡ $SONi^+$ dominates the retention in the pH range 6–9 while the ≡ SONiOH species governs the speciation above pH = 9. In agreement with the experimental results, no effect of carbonate complexation is predicted in the pH range up to 9. The parameters also allow representation of the data obtained with the R1 clay (Fig. 4).

3.3. From the clay fraction to the COX

The objective here is to assess the role of the clay fraction on Ni(II) adsorption in the presence of full-complexity COX rock samples. This has been analyzed by a modeling approach coupled with a spectroscopic investigation on our reference sample EST26480.

3.3.1. Quantitative description

Adsorption data were measured under the conditions representative of the COX formation (P_{CO2}, SPW) (Fig. 5A). Models 1 and 2 were first used with the 2SPNE SC model to predict the adsorption behavior considering competition between Ni(II) and trace elements for surface complexation sites. Iron(II) concentration, a key factor to consider in the approach (Bradbury and Baeyens, 2011), was fixed to the maximum value observed in the system (*i.e.* 10^{-6} M). The Fe(II) surface complexation constants were taken as the same as for Ni(II) (Bradbury and Baeyens, 2011). In agreement with the study realized with the <2 μm fraction, the result, represented by the dotted line in Fig. 5A, confirms that model 2 is inappropriate except for the highest concentrations. For $[Ni]_{eq.}$ < 5.10^{-6} M, the model is very sensitive to the competition effect on the strong site with Fe(II), as it was shown in (Bradbury and Baeyens, 2011). However, the consideration of the aqueous iron concentration measured at equilibrium is not sufficient to allow a good prediction of experimental data. In the concentration range between 5.10^{-6}

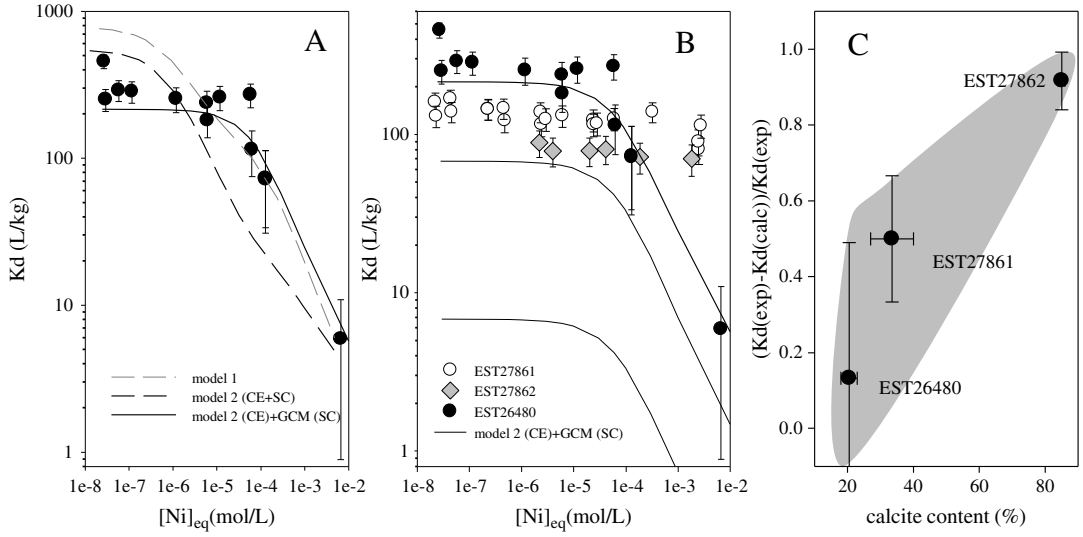

Fig. 5. Ni(II) adsorption on COX samples; effect of Ni(II) concentration; SPW, 1% CO_2 and S/L = 1 g/L; (A) models tested for the richest sample in clay (EST26480); (B) Experimental data for the three studied samples and prediction with the GCM (lines). (C) Quantification of the extra-adsorption (represented by the difference between the mean experimental (calculated from the data measured for $[Ni]_{eq.}$ < 10^{-5} M), Kd(exp), and the predicted Kd values, Kd(calc) over Kd(exp)) as a function of the calcite content. The lines in figure B and C correspond to the tested model with parameters given in Tables 1, 3, 4 and 5.

and 10^{-3} M where the surface complexation is governed by the weak site, the model significantly underestimates the retention. This cannot be explained by a competition effect, and this could be linked to an underestimation of the adsorption constant for the weak site, as pointed out in Section 3.2.1. Model 1 leads to a better prediction, expect at low Ni concentration. The better agreement between experimental results and calculated values was obtained when the GCM is used for describing the surface complexation reactions. In agreement with the data obtained for the Opalinus Clay (Bradbury and Baeyens, 2011), this result indicates that adsorption for our reference clay sample is controlled by the clay fraction. With respect to the modelling approach, the adsorption is controlled by both the weak site and the cationic exchange capacity in the Ni concentration range studied. No strong sites had to be considered, probably resulting from a blocking by competitive cations.

In the following, except where indicated, predictions will be made with model 2 (Table 4) and the GCM (Table 5) for describing the exchange and surface complexation reactions, respectively.

3.3.2. XPS

Samples were prepared with EST26480 and R0 under the experimental conditions necessary for detecting Ni(II) at the surface. The GCM predicts that Ni(II) sorbs on both the edges sites (as an inner-sphere complex) and within the interlayers (as an outer-sphere surface complex) in a similar proportion. Based on literature data (*e.g.* (Kowal-Fouchard et al., 2004)), the two different Ni(II) environments should result in two different binding energies / peaks in the XPS spectrum.

Oxygen 1 s spectra could be deconvoluted into two components (data not shown) at 530.4 eV and 531.6 eV. They can be assigned to Al_2O_3/SiO_2 (530.6 eV, (Liao et al., 1993) and 530.4 eV (Kaneko and Suginohara, 1978)) and OH (531.7 eV, (Lim and Atrens, 1990)), respectively. The positions are close to the reference values, indicating a good calibration of the system.

The XPS spectra obtained with Ni(II) are shown in Fig. 6. Only the Ni $2p_{3/2}$ photo peak could be detected for the Ni(II) metal ion loading studied. The spectra could be properly fitted considering one component and a satellite using a Gaussian–Lorentzian function with binding energies of 855.49/860.99 and 854.69/860.29 eV for R0 and EST26480, respectively. The photo peaks appear relatively broad (FWHMs of 2.5 eV and 2.8 V for Ni(II)-R0 and Ni(II)-EST26480, respectively) but no more than one surface species could be identified by fitting. This result is not consistent with the modeling approach which predicts at least two distinct environments. A similar result was observed for montmorillonite (Davison and McWhinnie, 1991); according to the model of Bradbury and Baeyens (1997) and the experimental conditions indicated in the paper, the sample should contain a mixture of Ni(II) sorbed on interlayers (87%) and on weak edge sites (13%). However, only one photo peak could be detected with a relatively high FWHM above 3.4 eV.

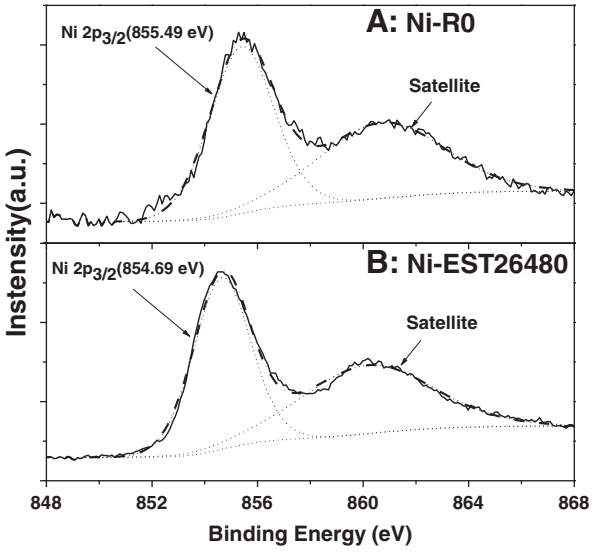

Fig. 6. XPS spectra and their decomposition for Ni(II)/R0 (A) and Ni(II)/EST26480 (B).

For R0, the binding energy falls in the 855–857.5 eV range suggesting an octahedral environment (Matienzo et al., 1973), as was observed for several clay minerals: hectorite (Davison and McWhinnie, 1991), rectorite (Tan et al., 2008) and montmorillonite (Davison and McWhinnie, 1991). A value about 0.8 eV lower was observed for the COX sample. The error in the estimation of the peak maximum ($\pm$0.3 eV) indicates a slightly different environment.

XPS results, therefore, suggest the existence of one octahedral environment (or at least an environments characterized by similar binding energies) which might be slightly different in COX and R0 samples. Scheidegger et al. (1998) showed that once Ni(II) is sorbed on clay and aluminium oxide mineral surfaces at relative high loading, a nucleation process (mixed Ni/Al phase formation) occurs. The presence of such a process would explain the presence of a single Ni(II) environment.

3.3.3. EXAFS

Normalized, background-subtracted and k^3-weighted spectra and corresponding Fourier transformed radial structure functions (RSFs) of Ni(II) sorbed on enriched clay fraction and COX are shown in Fig. 7. The spectra are uncorrected for phase shift. The k^3-weighted spectra (Fig. 7a) and corresponding RSFs (Fig. 7b) of Ni(II) sorbed on R0 and EST26480 are similar suggesting a similar environment.

The spectra were fitted considering the formation of a metal phyllosilicate. Based on the XPS results, the number of oxygens in the first coordination sphere was fixed at 6. Ni–Ni and Ni–Si subshells were considered to explain the peak at 2.9 Å (Fig. 7b). The parameters are identical within the error bars for both samples and agree with those obtained for model clay minerals (Dähn et al., 2002) (Table 6).

The formation of metal phyllosilicate appears to control the speciation of sorbed Ni(II) for the high metal ion loading studied by EXAFS. Therefore, the contribution of a nucleation processes in the modelling of adsorption data cannot be ignored. However, considering the relative good agreement between the experimental data and the adsorption model, one can assume that this process remains not significant in the range of Ni concentration studied by the batch method (Figs. 3 and 5).

Furthermore, the similitude of the EXAFS results obtained for Ni(II)/R0 and Ni(II)/EST26480 systems would confirm that Ni(II) interaction with the COX sample is governed by the clay fraction.

4. Effect of mineralogy

The variation in clay composition on the Ni adsorption was assessed in Section 3.2. The derived adsorption model allowed representation of Ni adsorption on the COX sample having the highest clay content. However, the clay content changes within the formation and can decrease to a few percent. Therefore we tested whether the clay fraction still dominates adsorption under these conditions. The results are presented in Fig. 5B.

As expected, the lower the content of clay, the lower the adsorption. The Kd value ranges from 60 to 300 L/kg. The GCM underestimates the adsorption for samples EST27861 and EST27862, and particularly for the one with the lowest clay content (0–3%): the model predicts low Kd but significant Kd values were measured. Furthermore, a constant Ni adsorption is observed over the entire Ni concentration range with no saturation effects. It clearly appears that a second adsorption mechanism must be involved.

As shown in Table 1, the clay content is correlated with the carbonate phase content (and more particularly with calcite), *i.e.* the higher the clay fraction, the lower the carbonate phase fraction. The origin of this extra-adsorption is therefore quite probably related to calcite. This is schematically depicted in Fig. 5C: the extra-adsorption, quantified by the difference between the mean experimental (calculated from the data measured for $[Ni]_{eq.} < 10^{-5}$ M) and predicted Kd values over the

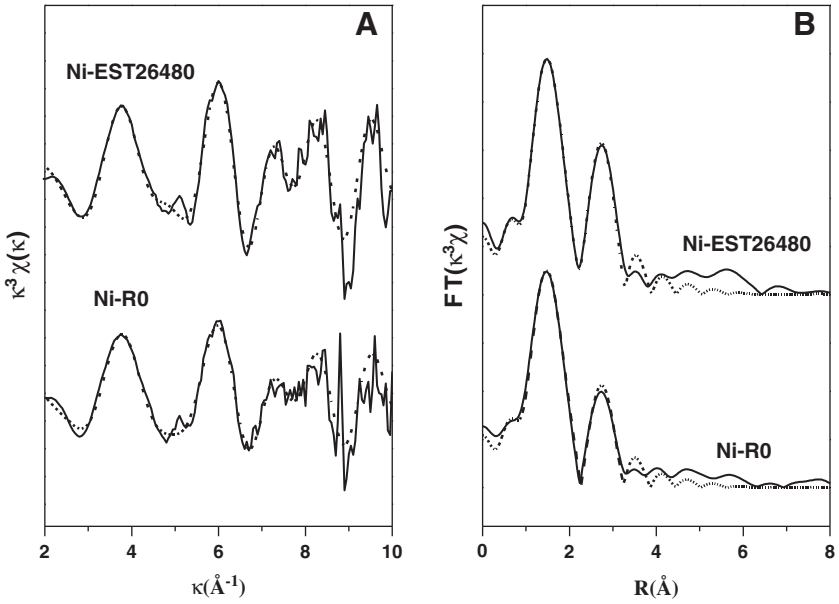

Fig. 7. k^3-weighted spectra (A) and radial structure functions (RSFs) obtained by forward Fourier transforms (uncorrected for phase shift) (B) for Ni(II)/R0 and Ni(II)/EST26480. The solid and dotted lines are fitted and experimental data, respectively.

experimental one, is nicely correlated with the calcite content. For EST26480, the extra-adsorption is equal to 0, within the experimental errors (*i.e.* the adsorption is controlled by the clay fraction) and becomes almost exclusive for sample EST27862.

For short contact times, as it is the case in the present study, Ni(II) adsorbs on calcite (Lakshtanov and Stipp, 2007). However, a simple adsorption process is not likely. First, considering the low specific surface of carbonate phases (~2–3 m^2/g) expected in the COX formation (ANDRA, 2012), and the site density proposed for calcite (Lakshtanov and Stipp, 2007), we expect a site concentration of about 1.8 10^{-5} mol/g for the COX sample with the highest content on carbonate phases (EST27862). This value cannot explain the constant adsorption observed in the Ni(II) concentration range studied (10^{-8}–10^{-4} M). Second, the model proposed in (Lakshtanov and Stipp, 2007) to describe Ni(II)/calcite interaction and used in the present case for the carbonate phases, give a Kd value of about 5 L/kg for sample EST27862 whereas a retention value around 60 L/kg was obtained.

Given the current state-of-knowledge, the mechanism at the origin of Ni(II) extra-adsorption appears unclear. An incorporation of Ni(II) into the calcite matrix seems to be unlikely as regards to the relatively short duration of the adsorption experiments. On the other hand, co-precipitation mechanism of nickel and divalent metals with calcite is also reported in the literature (Curti, 1999) and could constitute a plausible assumption explaining the extra adsorption of Ni(II) onto COX.

4.1. Conclusion

The "bottom-up" approach considering the clay fraction as a mixture of illite and montmorrilonite is appropriate for describing the cation exchange process on the clay-enriched <2 μm fraction with published parameters. However, a less good agreement was obtained between prediction and experimental results when the surface complexation mechanism considered within the 2 SPNE SC model is used. An operational approach based on the generalized composite model (GCM) was therefore proposed for describing Ni adsorption on COX. It corresponds basically to the model proposed for the Opalinus Clay (Bradbury and Baeyens, 2011) omitting the strong site and in which the surface complexation constants for the weak site have been adjusted to the experimental data without linking the reactivity strength with a pure model clay phase. The difficulty in generalizing the quantitative description of clay minerals reactivity with divalent metal ions was notably recently reviewed/discussed in Tournassat et al. (2013). Integrating this operational model into an additive approach taking into account clay mineralogy allows prediction of the behavior of Ni(II) on the representative COX sample having a relative high clay fraction (~50%). The crucial role of this clay fraction in the retention was confirmed at the molecular level by XPS and EXAFS for high Ni loadings where a nucleation process (formation of Ni phyllosilicate) appears to control Ni(II) adsorption on the samples. However, the model underestimates the retention when the clay content decreases, *i.e.* when the content in carbonate phases increases. It notably and largely underestimates the adsorption for the sample with the highest carbonate content (85%): whereas a significant adsorption is measured (Kd = 60 L/kg), the model predicts a adsorption of around 3 L/kg. Further experimental data will be necessary to understand the origin of this extra adsorption. A Kd range from 60 to 300 L/kg for trace concentrations of Ni(II) (~5.10^{-8}–10^{-5} M) is appropriate for clayrock having clay contents above 1.5%.

Acknowledgments

We thank ANDRA (ARMINES-NNPHY-00637) for the financial support given in the framework of the GL-Transfer Project, BRGM (Orléans,

Table 6
Structural parameters obtained from EXAFS analysis.

Sample	Ni–O shell			Ni–Ni shell			Ni–Si shell			Res%
	R(Å)	CN	σ^2	R(Å)	CN Å)	σ^2	R(Å)	CN	σ^2	%
R0 fraction R = 0	2.04	6.0[f]	0.009	3.06	2.8	0.008[f]	3.25	2.8	0.008[f]	0.29
EST26480	2.05	6.0[f]	0.008	3.08	3.8	0.008[f]	3.25	2.8	0.008[f]	0.02

R, interatomic distance; CN, coordination number; σ^2, Debye–Waller factor; Res, measure of the agreement between experimental and theoretical EXAFS curves. [f] Fixed value in the fitting; σ^2 values for Ni–Ni shell and Ni–Si shell were taken from (Dähn et al., 2002).

France) for providing us the <2 μm fractions and A. Bouchet (ERM, Orléans, France) for the mineralogical analysis. Thanks are also extended to Dr. S.T. Yang (Institute of Plasma Physics, China) and Dr J. Vandenborre (SUBATECH) for the valuable help for EXAFS and XPS data interpretation, respectively.

References

ANDRA, 2012. Dossier 2005 argile-Référentiel du site Meuse/Haute-Marne. TOME 1. ANDRA.

Ankudinov, A.L., Rehr, J.J., 1997. Relativistic calculations of spin-dependent X-ray-absorption spectra. J. Phys. Rev. B 56 (4), 1712–1716.

Bouchet, A., 1992. Mise au point d'un programme de détermination automatique des minéraux argileux. Comptes Rendus du Colloque de Rayons X-Siemens. 2, pp. 52–61.

Bradbury, M.H., Baeyens, B., 1997. A mechanistic description of Ni and Zn sorption on Na-montmorillonite Part II: modelling. J. Contam. Hydrol. 27 (3–4), 223–248.

Bradbury, M.H., Baeyens, B., 2000. A generalised sorption model for the concentration dependent uptake of caesium by argillaceous rocks. J. Contam. Hydrol. 42 (2–4), 141–163.

Bradbury, M.H., Baeyens, B., 2005a. Experimental measurements and modeling of sorption competition on montmorillonite. Geochim. Cosmochim. Acta 69 (17), 4187–4197.

Bradbury, M.H., Baeyens, B., 2005b. Modelling the sorption of Mn(II), Co(II), Ni(II), Zn(II), Cd(II), Eu(III), Am(III), Sn(IV), Th(IV), Np(V) and U(VI) on montmorillonite: linear free energy relationships and estimates of surface binding constants for some selected heavy metals and actinides. Geochim. Cosmochim. Acta 69 (4), 875–892.

Bradbury, M.H., Baeyens, B., 2009. Sorption modelling on illite Part I: Titration measurements and the sorption of Ni, Co, Eu and Sn. Geochim. Cosmochim. Acta 73 (4), 990–1003.

Bradbury, M., Baeyens, B., 2011. Predictive sorption modelling of Ni(II), Co(II), Eu(III), Th(IV) and U(VI) on MX-80 bentonite and Opalinus Clay: a "bottom-up" approach. Appl. Clay Sci. 52, 27–33.

Calvert, C.S., Palkowsky, D.A., Pevear, D.R., 1989. A combined X-ray powder diffraction and chemical method for the quantitative mineral analysis of geologic samples. In: Pevear, D.R., Mumpton, F.A. (Eds.), Quantitative Mineral Analysis of Clays vol. 1. Clay Minerals Society, pp. 154–167.

Claret, F., Sakharov, B.A., Drits, V.A., Velde, B., Meunier, A., Griffault, L., Lanson, B., 2004. Clay minerals in the Meuse-Haute Marne underground laboratory (France): possible influence of organic matter on clay mineral evolution. Clay Clay Miner. 52, 515–532.

Cosenza, P., Robinet, J.C., Pret, D., Huret, C., Fleury, M., Geraud, Y., Lebon, P., Villieras, F., Zamora, M., 2014. Indirect estimation of the clay content of clay-rocks using acoustic measurements: new insights from the deep borehole of Montiers-sur-Saulx (Meuse, France). Mar. Pet. Geol. 53, 117–132.

Curti, E., 1999. Coprecipitation of radionuclides with calcite: estimation of partition coefficients based on a review of laboratory investigations and geochemical data. Appl. Geochem. 14, 433–445.

Dähn, R., Scheidegger, A.M., Manceau, A., Schlegel, M.L., Baeyens, B., Bradbury, M.H., Morales, M., 2002. Neoformation of Ni phyllosilicate upon Ni uptake on montmorillonite: a kinetics study by powder and polarized extended X-ray absorption fine structure spectroscopy. Geochim. Cosmochim. Acta 66 (13), 2335–2347.

Davies, C.W., 1962. Ion Association. Butterworths.

Davis, J.A., Coston, J.A., Kent, D.B., Fuller, C.C., 1998. Application of the surface complexation concept to complex mineral assemblages. Environ. Sci. Technol. 32 (19), 2820–2828.

Davis, J.A., Meece, D.E., Kohler, M., Curtis, G.P., 2004. Approaches to surface complexation modeling of Uranium (VI) adsorption on aquifer sediments1. Geochim. Cosmochim. Acta 68 (18), 3621–3641.

Davison, N., McWhinnie, W.R., 1991. X-ray photoelectron spectroscopy study of Cobalt(II) and Nickel(II) sorbed on Hectorite and Montmorillonite. Clay Clay Miner. 39 (1), 22–27.

Deer, W.A., Howie, R.A., Zussman, J., 1992. An Introduction to the Rock-forming Mineral. Longman Scientific & Technical.

Donat, R., Akdogan, A., Erdem, E., Cetisli, H., 2005. Thermodynamics of Pb^{2+} and Ni^{2+} adsorption onto natural bentonite from aqueous solutions. J. Colloid Interface Sci. 286 (1), 43–52.

Duro, L., Grivé, M., Giffaut, E., 2012. ThermoChimie, the ANDRA Thermodynamic Database. MRS Spring Meeting. Materials Research Society.

Echeverría, J., Indurain, J., Churio, E., Garrido, J., 2003. Simultaneous effect of pH, temperature, ionic strength, and initial concentration on the retention of Ni on illite. Colloids Surf. A Physicochem. Eng. Asp. 218 (1–3), 175–187.

Elzinga, E.J., Sparks, D.L., 2001. Reaction condition effects on nickel sorption mechanisms in illite–water suspensions. Soil Sci. Soc. Am. J. 65 (1), 94–101.

Gaines, G.L., Thomas, H.C., 1953. Adsorption studies on clay minerals. 2: A formulation of the thermodynamics of exchange adsorption. J. Chem. Phys. 21 (4), 714–718.

Gaucher, E., Robelin, C., Matray, J.M., Négrel, G., Gros, Y., Heitz, J.F., Vinsot, A., Rebours, H., Cassagnabère, A., Bouchet, A., 2004. ANDRA underground research laboratory: interpretation of the mineralogical and geochemical data acquired in the Callovian–Oxfordian formation by investigative drilling. Phys. Chem. Earth 29, 55–77.

Gaucher, E., Blanc, P., Bardot, F., Braibant, G., Buschaert, S., Crouzet, C., Gautier, A., Girard, J.P., Jacquot, E., Lassin, A., Negrel, G., Tournassat, C., Vinsot, A., Altmann, S., 2006. Modelling the porewater chemistry of the Callovian–Oxfordian formation at a regional scale. C. R. Geosci. 338, 917–930.

Gaucher, E., Lerouge, C., Blanc, P., Tournassat, C., 2007. Caractérisation géochimique des forages PAC et nouvelles modélisations THERMOAR. BRGM.

Gaucher, E.C., Tournassat, C., Pearson, F., Blanc, P., Crouzet, C., Lerouge, C., Altmann, S., 2009. A robust model for pore-water chemistry of clayrock. Geochim. Cosmochim. Acta 73 (21), 6470–6487.

Gu, X., Evans, L.J., 2007. Modelling the adsorption of Cd(II), Cu(II), Ni(II), Pb(II), and Zn(II) onto Fithian illite. J. Colloid Interface Sci. 307 (2), 317–325.

Hartmann, E., Geckeis, H., Rabung, T., Lützenkirchen, J., Fanghänel, T., 2008. Sorption of radionuclides onto natural clay rocks. Radiochim. Acta 96, 699–707.

Hu, B., Cheng, W., Zhang, H., Yang, S., 2010. Solution chemistry effects on sorption behavior of radionuclide $^{63}Ni(II)$ in illite–water suspensions. J. Nucl. Mater. 406 (2), 263–270.

Hummel, W., Berner, U., Curti, E., Pearson, F.J., Thoenen, T., 2002. Nagra/PSI Chemical Thermodynamic Data Base 01/01. Universal-Publishers.

Kaneko, Y., Suginohara, Y., 1978. Observation of Si 2p binding energy by ESCA and determination of O^0, O^- and O^{2-} ions in silicate. J. Jpn. Inst. Metals 42 (3), 285–289.

Kowal-Fouchard, A., Drot, R., Simoni, E., Marmier, N., Fromage, F., Ehrhardt, J.J., 2004. Structural identification of europium(III) adsorption complexes on montmorillonite. New J. Chem. 28, 864–869.

Kraepiel, A.M.L., Keller, K., Morel, F.M.M., 1999. A model for metal adsorption on montmorillonite. J. Colloid Interface Sci. 210 (1), 43–54.

Lakshtanov, L.Z., Stipp, S.L.S., 2007. Experimental study of nickel(II) interaction with calcite: adsorption and coprecipitation. Geochim. Cosmochim. Acta 71 (15), 3686–3697.

Lanson, B., Bouchet, A., 1995. Identification des minéraux argileux par diffraction des rayons X: apport du traitement numérique. Bull. Centres Rech. Explor. Prod. Elf-Aquitaine 19, 91–118.

Liao, H.M., Sodhi, R.N.S., Coyle, T.W., 1993. Surface composition of AlN powders studied by X-ray photoelectron spectroscopy and bremsstrahlung-excited Auger electron spectroscopy. J. Vac. Sci. Technol. A: Vacuum Surf. Films 11 (5), 2681–2686.

Lim, A.S., Atrens, A., 1990. ESCA studies of nitrogen-containing stainless steels. Appl. Phys. A Mater. Sci. Process. 51 (5), 411–418.

Ma, C., Eggleton, R.A., 1999. Cation exchange capacity of kaolinite. Clay Clay Miner. 47, 174–180.

Maes, N., Salah, S., Jacques, D., Aertsens, M., Van Gompel, M., De Cannière, P., Velitchkova, N., 2008. Retention of Cs in boom clay: comparison of data from batch sorption tests and diffusion experiments on intact clay cores. Phys. Chem. Earth 33 (Supplement 1), S149–S155.

Matienzo, L.J., Yiu, L.T., Grim, S.O., Schwartz Jr., W.E., 1973. X-ray photoelectron spectroscopy of nickel compounds. Inorg. Chem. 12, 2762–2769.

Newman, A.C.D., Brown, G., 1987. The chemical constitution of clays. In: Newman, A.C.D. (Ed.), Chemistry of Clays and Clay Minerals. Mineralogical Society, pp. 1–128.

Parkhurst, D.L., Appelo, C.A.J., 1999. User's guide to Phreeqc (version 2) _ A computer program for speciation, batch reaction, one-dimensional transport, and inverse geochemical calculations. USGS, p. 312, Report 99-4259.

Ravel, B., Newville, M., 2005. ATHENA, ARTEMIS, HEPHAESTUS: data analysis for X-ray absorption spectroscopy using IFEFFIT. J. Synchrotron Radiat. 12 (4), 537–541.

Rémy, J.C., Orsini, L., 1976. Utilisation du chlorure de cobaltihexamine pour la détermination simultanée de la capacité d'échange et des bases échangeables dans les sols. Sciences du Sol 4, 269–275.

Reynolds, R.C., 1980. Interstratified clay minerals. In: Brindley, G.W., Brown, G. (Eds.), Crystal Structures of Clay Minerals and Their X-ray Identification. Mineralogical Society, pp. 249–304.

Robert, M., 1996. Le sol: interface dans l'environnement, ressource pour le développement. Masson.

Scheidegger, A.M., Strawn, D.G., Lamble, G.M., Sparks, D.L., 1998. The kinetics of mixed Ni–Al hydroxide formation on clay and aluminum oxide minerals: a time-resolved XAFS study. Geochim. Cosmochim. Acta 62 (13), 2233–2245.

Song, X., Wang, S., Chen, L., Zhang, M., Dong, Y., 2009. Effect of pH, ionic strength and temperature on the sorption of radionickel on Na-montmorillonite. Appl. Radiat. Isot. 67 (6), 1007–1012.

Tan, X., Chen, C., Yu, S., Wang, X., 2008. Sorption of Ni^{2+} on Na-rectorite studied by batch and spectroscopy methods. Appl. Geochem. 23 (9), 2767–2777.

Tertre, E., Berger, G., Castet, S., Loubet, M., Giffaut, E., 2005. Experimental sorption of Ni^{2+}, Cs^{+} and Ln^{3+} onto a montmorillonite up to 150 °C. Geochim. Cosmochim. Acta 69 (21), 4937–4948.

Tertre, E., Hofmann, A., Berger, G., 2008. Rare earth element sorption by basaltic rock: experimental data and modeling results using the "Generalised Composite approach". Geochim. Cosmochim. Acta 72 (4), 1043–1056.

Tournassat, C., Gaucher, E.C., Fattahi, M., Grambow, B., 2007. On the mobility and potential retention of iodine in the Callovian–Oxfordian formation. Phys. Chem. Earth Parts A/B/C 32 (8), 539–551.

Tournassat, C., Gailhanou, H., Crouzet, C., Braibant, G., Gautier, A., Gaucher, E.C., 2009. Cation exchange selectivity coefficient values on smectite and mixed-layer illite/smectite minerals. Soil Sci. Soc. Am. J. 73 (3), 928–942.

Tournassat, C., Grangeon, S., Leroy, P., Giffaut, E., 2013. Modeling specific pH dependent sorption of divalent metals on Montmorillonite surfaces. A review of pitfalls, recent achievements and current challenges. Am. J. Sci. 313, 395–451.

Van Loon, L.R., Baeyens, B., Bradbury, M.H., 2009. The sorption behaviour of caesium on Opalinus Clay: a comparison between intact and crushed material. Appl. Geochem. 24 (5), 999–1004.

Vinsot, A., Linard, Y., Lundy, M., Altmann, S., 2010. Expérimentation POX, installation et premiers résultats. ANDRA.

Weaver, C.E., 1989. Clays, Muds and Shales. Elsevier.